Developments and Opportunities Related to High-Order Methods and Aerodynamic Shape Optimization

David W. Zingg
J. Armand Bombardier Foundation Chair in Aerospace Flight
Director, Institute for Aerospace Studies
University of Toronto

NASA Ames Research Center

July 14, 2015

Thanks to

- Dr. David Del Rey Fernandez, David Boom, Dr. Jason Hicken, Tom Reist, Dr. Hugo Gagnon
- Tom Pulliam, NASA
- Cetin Kiris

Topics

- Summation-by-parts operators on simplices
- Exploratory aerodynamic shape optimization
  - ★ application to a regional class blended wing-body aircraft

High-Order Methods

- Potentially efficient for a wide range of problems
  - Lower cost for a given accuracy
  - High order preferred primarily when error tolerance is tight
  - Singularities and discontinuities are an issue
  - Robustness is an issue
- Wide range of high-order methods available
  - Finite difference, finite element, finite volume, spectral difference, spectral element, spectral volume
  - Much current interest in discontinuous Galerkin and flux reconstruction methods

Properties of High-Order Methods

- Traditional implementation of finite difference methods
  - Repeating interior operator
  - Fixed number of boundary operators under refinement
  - Kronecker products in multiple dimensions
  - Curvilinear coordinate transformation
  - Mesh smoothness requirements
  - Very efficient
- Element type methods
  - applicable to unstructured grids
  - with interior degrees of freedom do not rely on mesh smoothness
  - amenable to h and p refinement

Summation by Parts

- Enables construction of operators with provable time stability
- Usually used with simultaneous approximation terms
- Usually used with finite-difference operators with a repeating interior operator on a uniform mesh
- Other known operators possess the SBP property (Carpenter and Gottlieb, Gassner)
- Recently generalized by Del Rey Fernández et al. to apply to nonuniform nodal distributions and element-type operators

Opportunities

- Combining the concept of a generalized SBP operator with the idea of implementing SBP operators as elements provides a basis for the development of SBP operators in multiple dimensions applicable to unstructured grids
- Very general approach to the construction of stable operators for unstructured grids
- Potential to lead to novel operators with useful properties
- Generality can be exploited to construct methods with specific properties (with provable time stability by construction)

Summation by Parts Operators: Definitions

$$H\delta_x u = Su \ , \qquad \text{i.e.} \ \frac{\partial \mathcal{U}}{\partial x} \approx Du = H^{-1}Su$$

where H is a diagonal SPD matrix that defines an inner product, norm, and quadrature by

$$(u,v)_H = u^T H v \ , \quad ||u||_H^2 = u^T H u \ , \quad \int_{x_\mathrm{L}}^{x_\mathrm{R}} \mathcal{U} \mathrm{d}x \approx \mathbf{1}^T H \boldsymbol{u}$$

and

$$S + S^T \ = \ E$$

where E depends on whether or not the nodal distribution, which can be nonuniform, includes the boundary nodes

Application to a PDE

Linear advection equation:

$$\frac{\partial \mathcal{U}}{\partial t} + \frac{\partial \mathcal{U}}{\partial x} = 0 \ , \qquad 0 \le x \le 1 \ , \qquad \mathcal{U}(0,t) = \mathcal{U}_L(t)$$

Discretize in space on a possibly nonuniform mesh with n nodes to obtain the semi-discrete form

$$\frac{\mathrm{d}u}{\mathrm{d}t} = Au - f(t)$$

where $u = [u_1, u_1, \dots, u_n]^T$
Matrix A includes contribution from treatment of boundary condition; will use SATs here with $\sigma_L = -1$ (later for element coupling will use SATs with $\sigma_L = -1/2$, $\sigma_R = 1/2$)
Time stable if all eigenvalues of A have real parts less than or equal to zero (for A nondefective)

A classical finite-difference SBP operator ($p = 2$)

$$D = H^{-1} S$$

Gives a second-order approximation to the first derivative (at the boundary nodes), which will lead to third-order solution to the linear convection equation

$$H = \Delta x \begin{bmatrix} h_{11} & & & & & \\ & h_{22} & & & & \\ & & h_{33} & & & \\ & & & h_{44} & & \\ & & & & 1 & \\ & & & & & \ddots \end{bmatrix}$$

$$S = \begin{bmatrix} -1/2 & S_{12} & S_{13} & S_{14} & & & & \\ -S_{12} & 0 & S_{23} & S_{24} & & & & \\ -S_{13} & -S_{23} & 0 & S_{34} & -1/12 & & & \\ -S_{14} & -S_{24} & -S_{34} & 0 & 8/12 & -1/12 & & \\ 0 & 0 & 1/12 & -8/12 & 0 & 8/12 & -1/12 & \\ & & & \ddots & \ddots & \ddots & \ddots & \ddots \end{bmatrix}$$

Resulting A matrix when implemented in the traditional finite-difference manner

$$A = (n-1)\begin{bmatrix}
\boxed{-\frac{24}{17}} & -\frac{59}{34} & \frac{4}{17} & \frac{3}{34} & & & & & & & \\
\frac{1}{2} & 0 & -\frac{1}{2} & 0 & & & & & & & \\
-\frac{4}{43} & \frac{59}{86} & 0 & -\frac{59}{86} & \frac{4}{43} & & & & & & \\
-\frac{3}{98} & 0 & \frac{59}{98} & 0 & -\frac{32}{49} & \frac{4}{49} & & & & & \\
 & & -\frac{1}{12} & \frac{2}{3} & 0 & -\frac{2}{3} & \frac{1}{12} & & & & \\
 & & & \ddots & \ddots & \ddots & \ddots & \ddots & & & \\
 & & & & -\frac{1}{12} & \frac{2}{3} & 0 & -\frac{2}{3} & \frac{1}{12} & & \\
 & & & & & -\frac{4}{49} & \frac{32}{49} & 0 & -\frac{59}{98} & 0 & \frac{3}{98} \\
 & & & & & & -\frac{4}{43} & \frac{59}{86} & 0 & -\frac{59}{86} & \frac{4}{43} \\
 & & & & & & & 0 & \frac{1}{2} & 0 & -\frac{1}{2} \\
 & & & & & & & -\frac{3}{34} & -\frac{4}{17} & \frac{59}{34} & -\frac{24}{17}
\end{bmatrix}$$

Finite-Difference Operators Implemented as Elements

$$A = \begin{bmatrix} \hat{\mathrm{A}} & \mathrm{SAT}_R & & & \\ \mathrm{SAT}_L & \tilde{A} & \mathrm{SAT}_R & & \\ & \ddots & \ddots & \ddots & \\ & & \mathrm{SAT}_L & \tilde{A} & \mathrm{SAT}_R \\ & & & \mathrm{SAT}_L & \breve{\mathrm{A}} \end{bmatrix}$$

where

$$\tilde{A} = \frac{8}{N} \begin{bmatrix} 0 & -\frac{59}{34} & \frac{4}{17} & \frac{3}{34} & & & & & \\ \frac{1}{2} & 0 & -\frac{1}{2} & 0 & & & & & \\ -\frac{4}{43} & \frac{59}{86} & 0 & -\frac{59}{86} & \frac{4}{43} & & & & \\ -\frac{3}{98} & 0 & \frac{59}{98} & 0 & -\frac{32}{49} & \frac{4}{49} & & & \\ & & -\frac{1}{12} & \frac{2}{3} & 0 & -\frac{2}{3} & \frac{1}{12} & & \\ & & & -\frac{4}{49} & \frac{32}{49} & 0 & -\frac{59}{98} & 0 & \frac{3}{98} \\ & & & & -\frac{4}{43} & \frac{59}{86} & 0 & -\frac{59}{86} & \frac{4}{43} \\ & & & & & 0 & \frac{1}{2} & 0 & -\frac{1}{2} \\ & & & & & -\frac{3}{34} & -\frac{4}{17} & \frac{59}{34} & 0 \end{bmatrix}$$

Generalized SBP example: nonuniform nodal distribution

Hybrid Gauss-trapezoidal-Lobatto quadrature nodal distribution given for 9 nodes by:

$$x = \frac{1}{8}\begin{bmatrix} 0 & \frac{12}{13} & 2 & 3 & 4 & 5 & 6 & (8-\frac{12}{13}) & 8 \end{bmatrix}^{\mathrm{T}}$$

$$D = 8\begin{bmatrix}
-\frac{864}{553} & \frac{408811}{209034} & -\frac{2901}{7742} & -\frac{278}{14931} & & & & & \\
-\frac{41}{78} & 0 & \frac{15}{26} & -\frac{2}{39} & & & & & \\
\frac{967}{7932} & -\frac{49855}{71388} & 0 & \frac{11800}{17847} & -\frac{56}{661} & & & & \\
\frac{139}{23460} & \frac{9971}{164220} & -\frac{1770}{2737} & 0 & \frac{1296}{1955} & -\frac{162}{1955} & & & \\
 & & \frac{1}{12} & -\frac{2}{3} & 0 & \frac{2}{3} & -\frac{1}{12} & & \\
 & & & \frac{162}{1955} & -\frac{1296}{1955} & 0 & \frac{1770}{2737} & -\frac{9971}{164220} & -\frac{139}{23460} \\
 & & & & \frac{56}{661} & -\frac{11800}{17847} & 0 & \frac{49855}{71388} & -\frac{967}{7932} \\
 & & & & & \frac{2}{39} & -\frac{15}{26} & 0 & \frac{41}{78} \\
 & & & & & \frac{278}{14931} & \frac{2901}{7742} & -\frac{408811}{209034} & \frac{864}{553}
\end{bmatrix}$$

Can be implemented in the traditional manner or as an element of size ≥ 9

Second generalized SBP example: fixed element size

Diagonal-norm operator on Chebyshev-Gauss-Lobatto quadrature nodal distribution given for 5 nodes by:

$$x = \frac{1}{2}\left[\begin{array}{ccccc} -1 & -\frac{1}{2}\sqrt{2} & 0 & \frac{1}{2}\sqrt{2} & 1 \end{array}\right]^{\mathrm{T}} + \left(\frac{1}{2}\right)\mathbf{1}$$

where $\mathbf{1}$ is a vector of ones

$$D = 2\begin{bmatrix} -\frac{15}{2} & 8+2\sqrt{2} & -6 & 8-2\sqrt{2} & -\frac{5}{2} \\ -1-\frac{1}{4}\sqrt{2} & 0 & \frac{3}{2}\sqrt{2} & -\sqrt{2} & 1-\frac{1}{4}\sqrt{2} \\ \frac{1}{2} & -\sqrt{2} & 0 & \sqrt{2} & -\frac{1}{2} \\ -1+\frac{1}{4}\sqrt{2} & \sqrt{2} & -\frac{3}{2}\sqrt{2} & 0 & 1+\frac{1}{4}\sqrt{2} \\ \frac{5}{2} & -8+2\sqrt{2} & 6 & -8-2\sqrt{2} & \frac{15}{2} \end{bmatrix}$$

Can only be implemented as an element

Intermediate Summary

- Have shown that SBP operators normally implemented in the traditional finite difference manner can also be implemented as elements
- Have shown examples of generalized SBP operators, some of which can only be implemented as elements
- These are not finite-element methods in the strict sense, as they do not have explicit bases
- This generality can be exploited to construct new methods with specific properties (with provable time stability by construction)

Multidimensional SBP Operators for Unstructured Grids

The matrix D_x is a degree p SBP approximation to the first derivative $\frac{\partial}{\partial x}$ if

1. $\mathsf{D}_x \boldsymbol{x}^{a_x} \circ \boldsymbol{y}^{a_y} = a_x \boldsymbol{x}^{a_x - 1} \circ \boldsymbol{y}^{a_y}, \ \forall\ a_x + a_y \leq p$;
2. $\mathsf{D}_x = \mathsf{H}^{-1}\mathsf{S}_x = \mathsf{H}^{-1}\left(\mathsf{Q}_x + \frac{1}{2}\mathsf{E}_x\right)$,
   where Q_x is antisymmetric, and E_x is symmetric;
3. H is symmetric positive definite, and;
4. $$\left(\boldsymbol{x}^{a_x} \circ \boldsymbol{y}^{a_y}\right)^{\mathrm{T}} \mathsf{E}_x \boldsymbol{x}^{b_x} \circ \boldsymbol{y}^{b_y} = \oint_{\Gamma} x^{a_x + b_x} y^{a_y + b_y} n_x \mathrm{d}\Gamma,$$
   $$\forall\ a_x + a_y,\, b_x + b_y \leq \tau_{\mathsf{E}_x}$$
   where $\tau_{\mathsf{E}_x} \geq p$ and $\boldsymbol{n} = [n_x, n_y]^{\mathrm{T}}$ is the outward pointing unit normal to the surface Γ.

The existence of diagonal-norm SBP operators is tied to the existence of a cubature rule

Theorem: Existence of an SBP operator

If the generalized Vandermonde matrix has full rank on the node set $\{(x_i, y_i)\}_{i=1}^{n}$, the existence of a cubature rule of degree $\tau \geq 2p - 1$ with positive weights is necessary and sufficient for the existence of degree p diagonal-norm SBP operators approximating the first derivatives $\frac{\partial}{\partial x}$ and $\frac{\partial}{\partial y}$ on the same nodes.

We have constructed simplex SBP operators from existing cubature rules

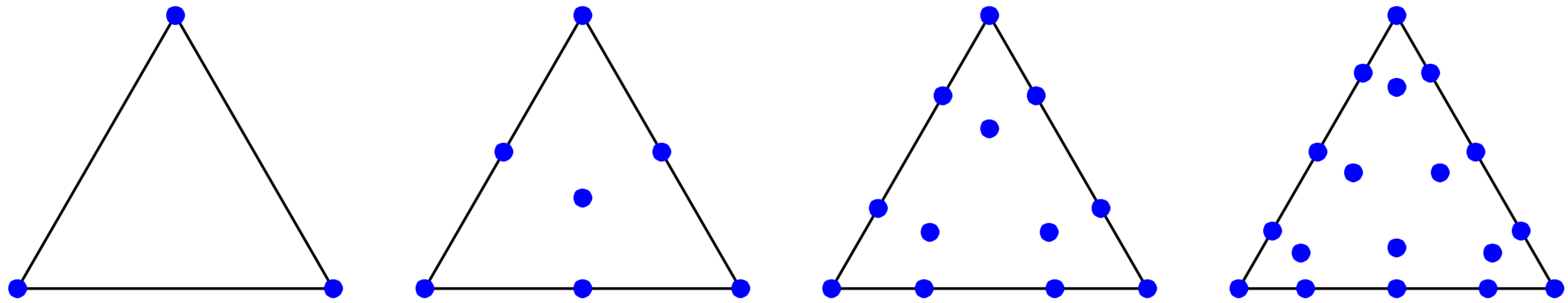

$p = 1$, 3 nodes | $p = 2$, 7 nodes | $p = 3$, 12 nodes | $p = 4$, 18 nodes

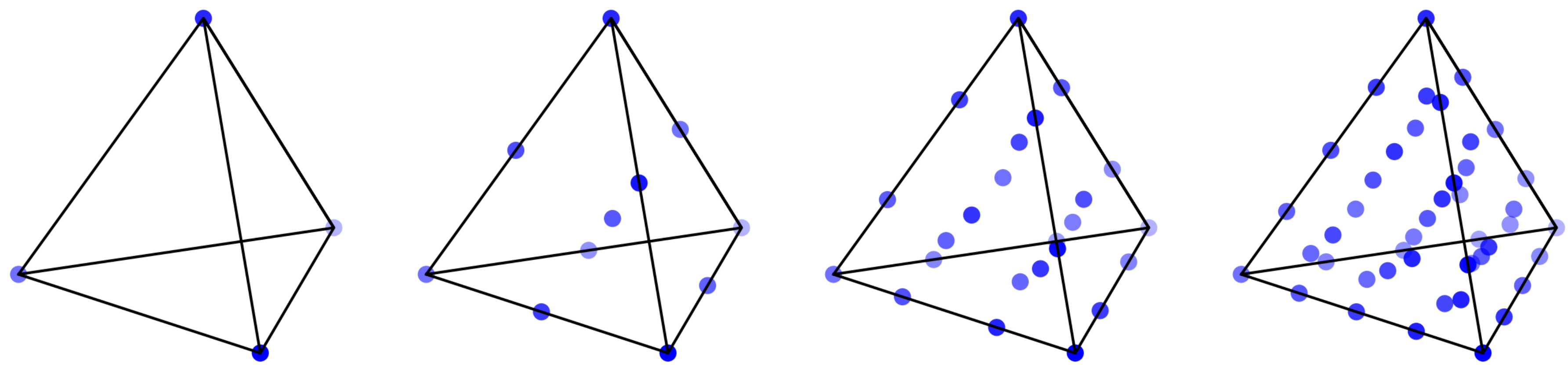

$p = 1$, 4 nodes | $p = 2$, 11 nodes | $p = 3$, 24 nodes | $p = 4$, 45 nodes

https://github.com/OptimalDesignLab/SummationByParts.jl

We verify the triangular SBP operators using the two-dimensional linear convection equation on a periodic domain

$$\frac{\partial \psi}{\partial t} + \boldsymbol{u} \cdot \nabla \psi = 0, \qquad \forall\, (x, y) \in [0, 1]^2,$$

$$\psi(x, 0, t) = \psi(x, 1, t), \qquad \text{and} \qquad \psi(0, y, t) = \psi(1, y, t),$$

$$\psi(x, y, 0) = \frac{1}{4}\left(3 - \cos(2\pi x)\right)\left(3 - \cos(2\pi y)\right).$$

- The advection velocity is $\boldsymbol{u} = (1, 1)$
- RK4 is used for the time-marching scheme

The square domain is divided into $2N^2$ triangular elements

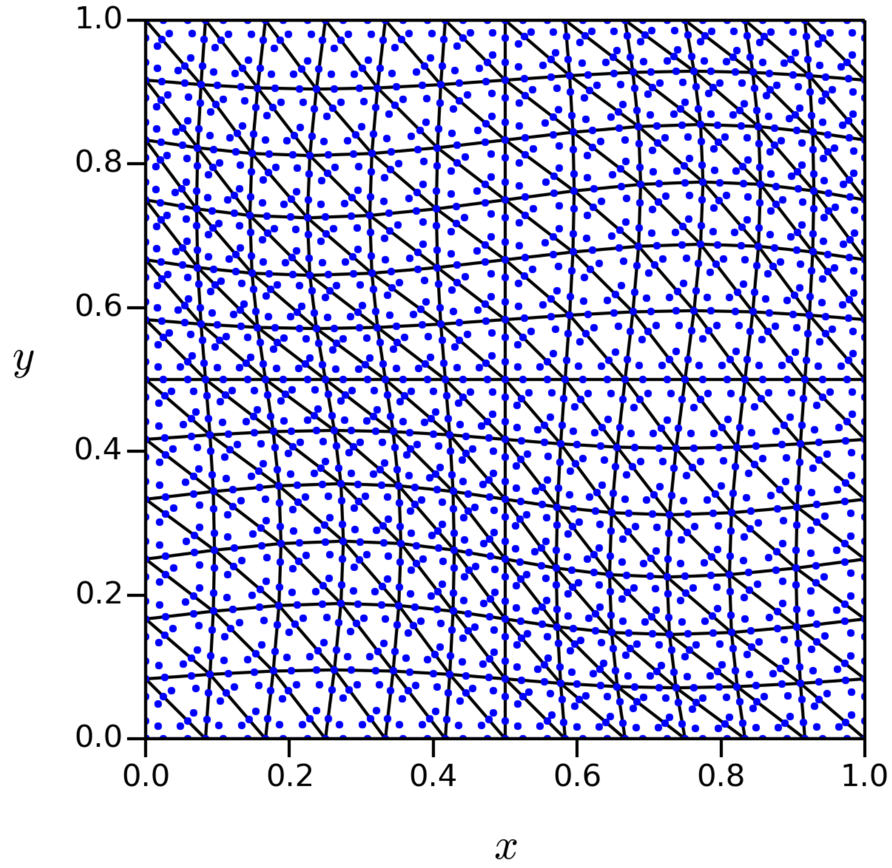

- N is the number of edges along one side of the domain
- a smooth perturbation is applied to the mesh vertices
- global SBP operators are constructed using the proposed assembly process

The L^2 solution error after one period for a range of $h = 1/N$

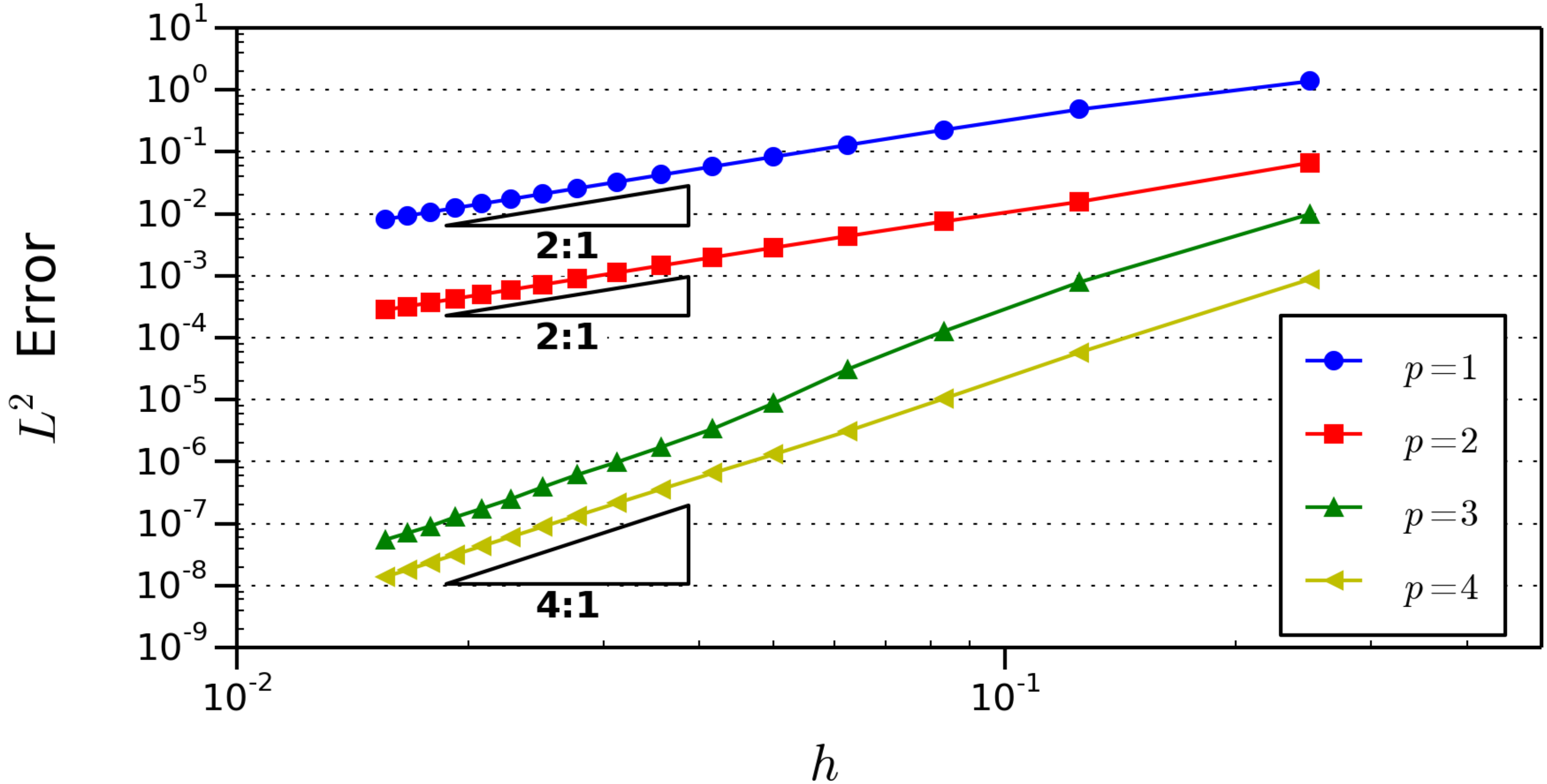

- even-p operators have lower than expected asymptotic rates

The high-order SBP operators are more efficient when high accuracy is necessary

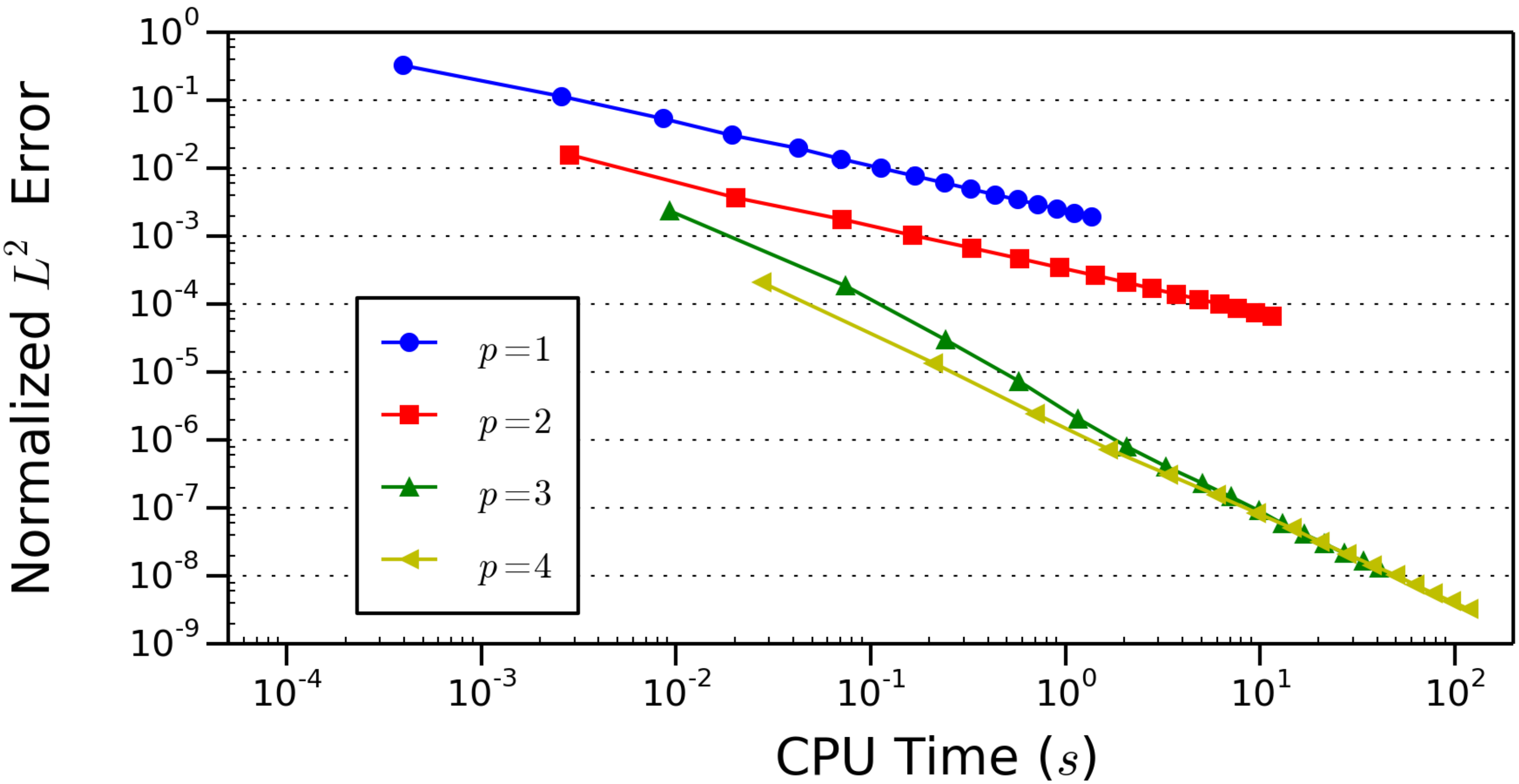

The spectrum of the SBP-discretized operator $\boldsymbol{u} \cdot \nabla$ has machine-zero real part

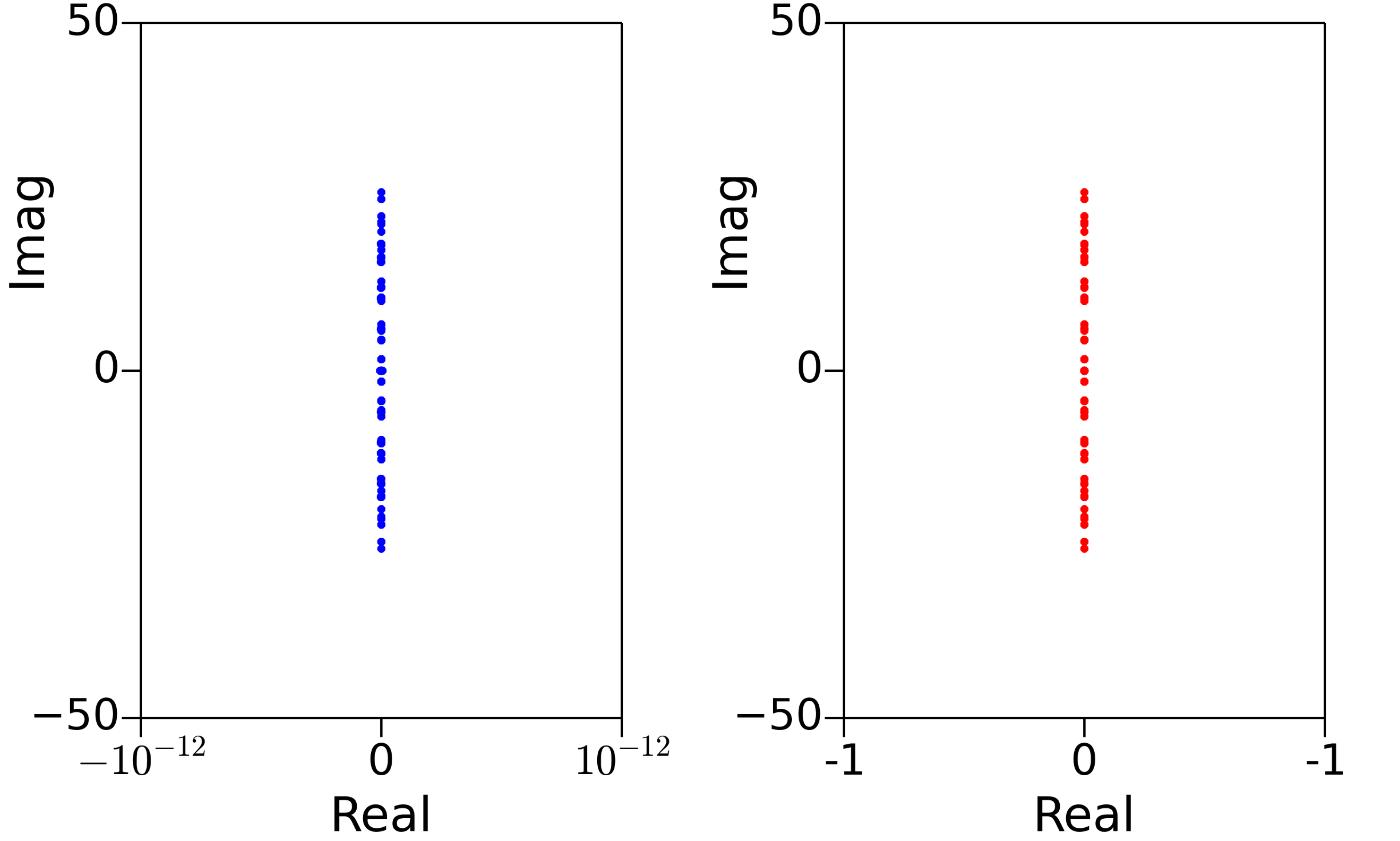

$p = 1$ (SBP) $\quad$ $p = 1$ (SE)

The spectrum of the SBP-discretized operator $\boldsymbol{u} \cdot \nabla$ has machine-zero real part

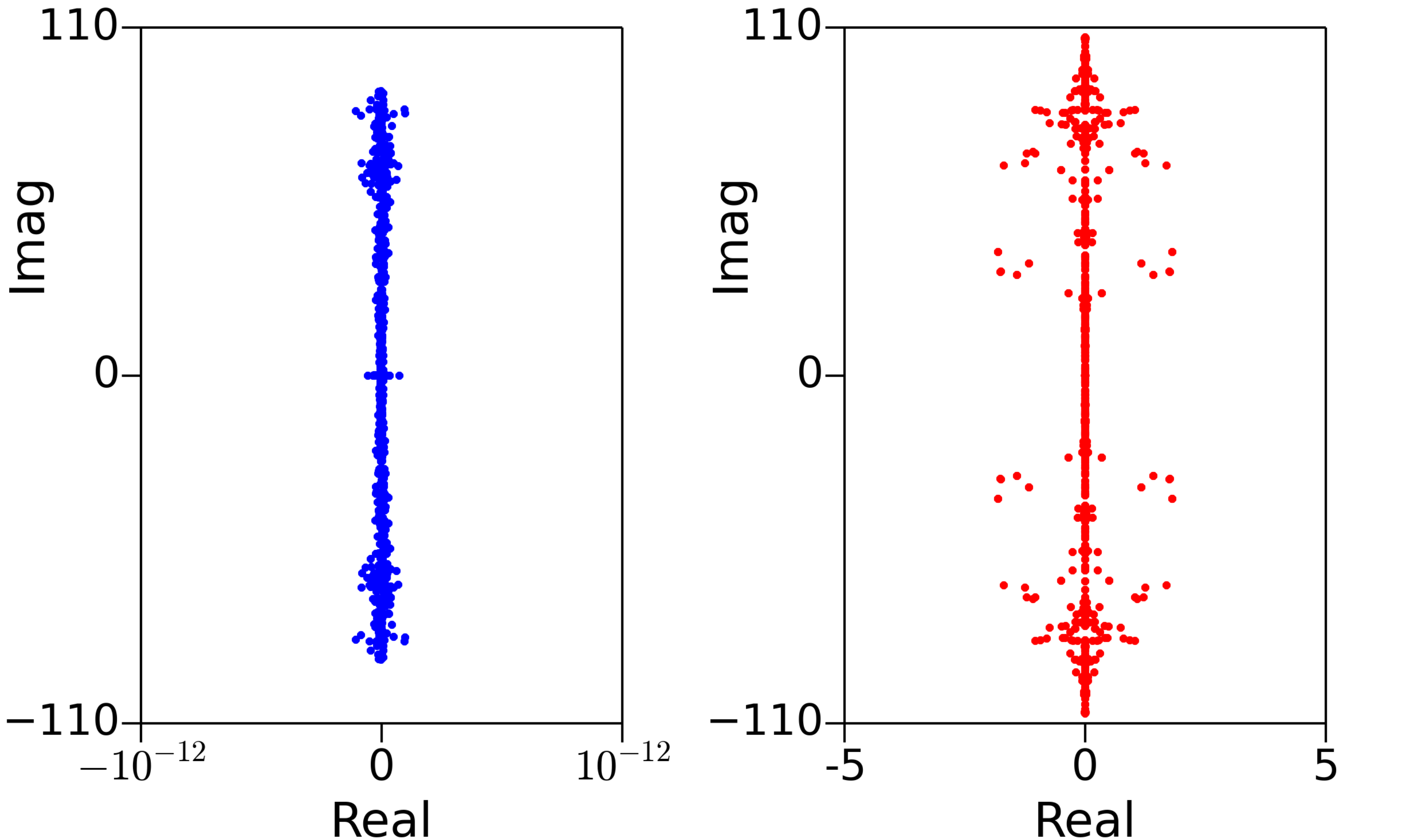

$p = 2$ (SBP) $\quad$ $p = 2$ (SE)

Summary

SBP operators offer discretizations with

- high-order accuracy,
- efficiency,
- stability.

A distinguishing feature of SBP operators is the flexibility in their construction, so they can be tailored to particular problem classes.

Exploratory Aerodynamic Shape Optimization

- numerical optimization is a powerful tool that enables:
  - ★ optimization and assessment of novel configurations and advanced aerodynamic concepts
  - ★ optimization of parameters in flow control strategies
  - ★ possible invention of hitherto unknown configurations or concepts

What is exploratory aerodynamic shape optimization?

	Conceptual design	Detailed design	Exploratory optimization
Comprehensive	✔	✔	✘
Large geometric variation	✔	✘	✔
High fidelity	✘	✔	✔

Applying Exploratory Aerodynamic Shape Optimization to Unconventional Aircraft Configurations

- in the evaluation of new concepts such as unconventional aircraft configurations it is critical that the concepts be optimized before comparisons are made
- this requires that preconceived notions of geometry be discarded as much as possible as well as previous design experience (which may not be applicable), leaving the optimizer as free as possible
- input from the designer should be limited to objectives, constraints, and performance requirements

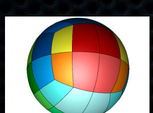

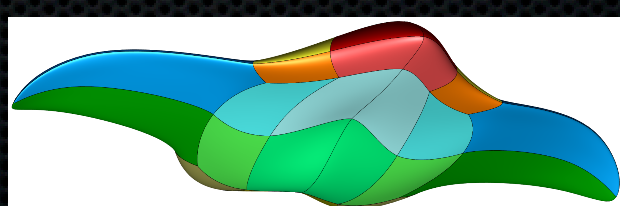
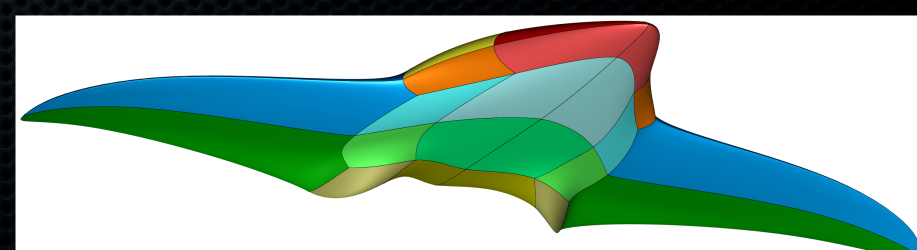

Components of Jetstream Aerodynamic Shape Optimization Methodology

- Efficient and robust flow solver for Euler and Reynolds-averaged Navier-Stokes equations: Diablo
  - ★ parallel implicit Newton-Krylov-Schur algorithm using summation-by-parts method for spatial discretization
- Adjoint method for gradient computation
- B-spline surface geometry parameterization
- Free form deformation or B-spline geometry control
- Integrated mesh movement technique based on B-spline volumes
- Sequential quadratic programming method for gradient-based optimization

Axial Deformation Tailored to Generic Wing Systems

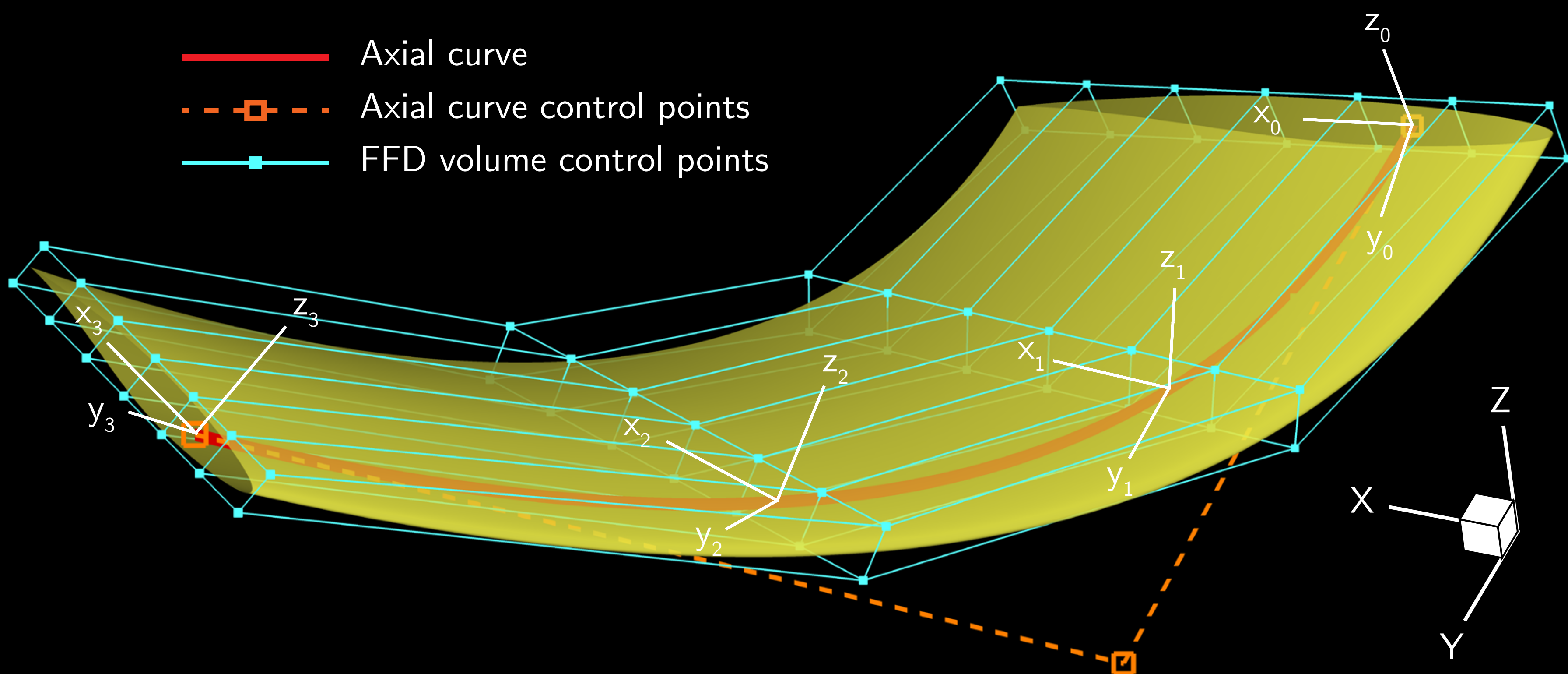

NURBS curves as axial curves: $\mathbf{C}^w(\xi) = \sum_{i=0}^{N} \mathcal{N}_i^{(p)}(\xi)\mathbf{P}_i^w$

The Blended Wing-Body (BWB)

Advantages:

- Aerodynamic
  - High wetted aspect ratio gives high lift-to-drag ratio
  - Natural ‘area-ruling’ improves high-speed performance
- Structural
  - Natural spanloading reduces bending loads
- Propulsive
  - Boundary-layer ingesting engines reduce fuel-burn
- Acoustic
  - Body-mounted engines are acoustically shielded
  - Low landing speed reduces airframe noise

Challenges:

- Aerodynamic
  - Shock-free airfoils with sufficient thickness
  - Maintaining stability and control without an empennage
- Structural
  - Design of non-cylindrical pressure vessel for the cabin
  - More complicated load-paths
- Propulsive
  - Robust boundary-layer ingesting engine technology
- Passenger comfort
  - Ride quality

Design Problem

- Investigate minimum drag potential of a regional jet
- Similar to the Embraer E190
  - 100 passengers
  - 2,000 nmi max range
  - 500 nmi nominal range
  - Cruise speed of Mach 0.78
  - Cruise altitude of 36,000 ft
- All designs sized using a low-fidelity conceptual design tool

Baseline Blended Wing-Body (BWB)

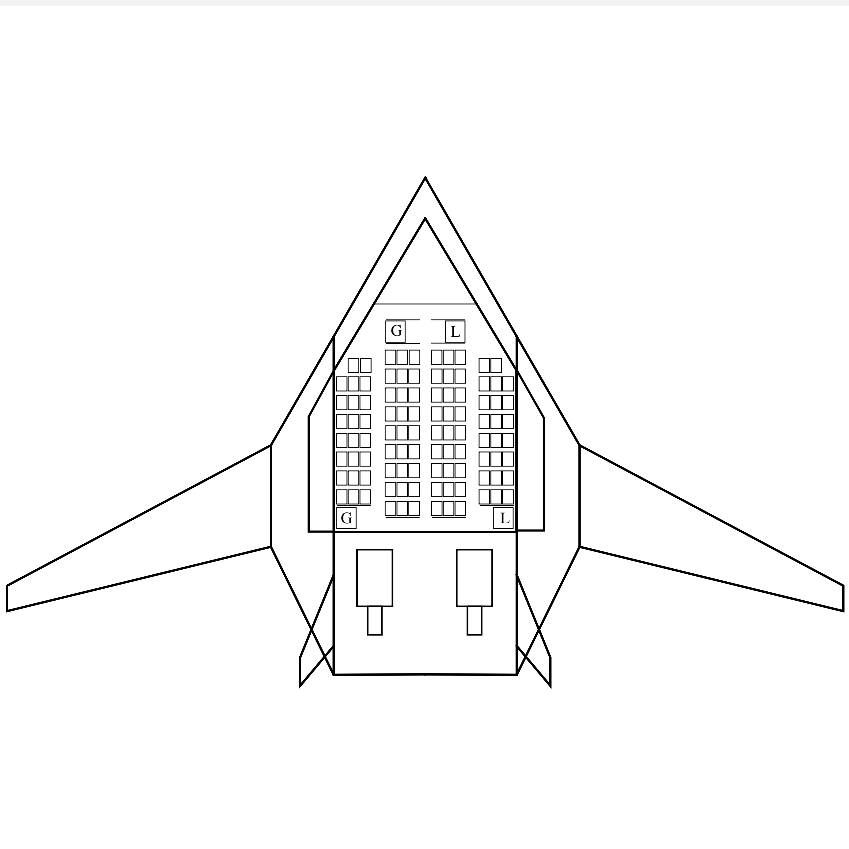

BWB100-02

Capacity		
Passengers + crew	100+5	
Max payload	28,400	lb
Geometry		
Reference area	2,734	ft^2
Total span	118	ft
Length	70	ft
MAC	42.4	ft
Aspect ratio	5.1	
Weight		
MTOW	119,700	lb
OEW	69,800	lb
Wing load at MTOW	43.8	lb/ft^2
Nominal mission cruise		
Range	500	nmi
Altitude	36,000	ft
Mach number	0.78	
Reynolds number	76	$\times 10^6$
Weight*	104,600	lb
C_L*	0.19	
CG location*	41	ft

* At start of cruise

Optimization Definition

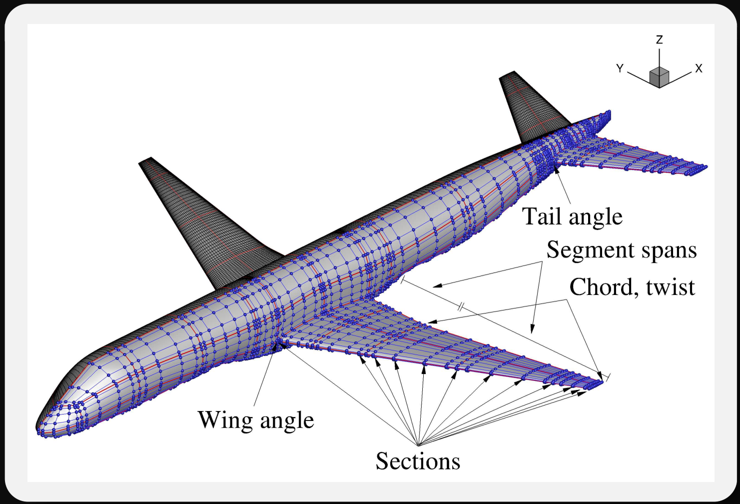

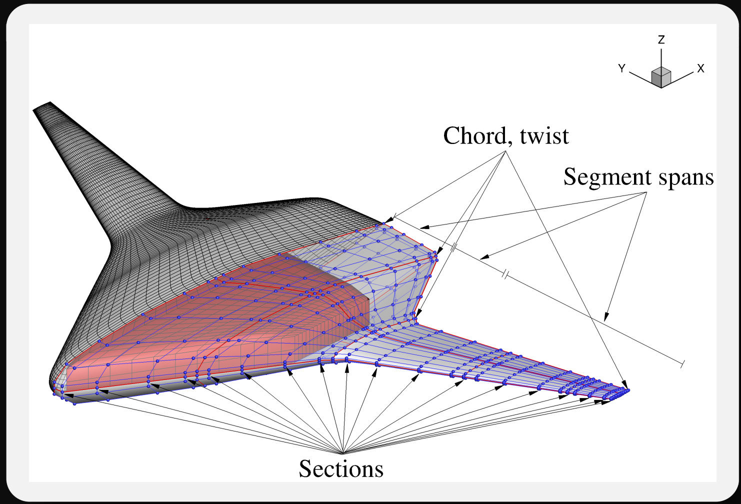

- Trim-constrained drag-minimization

- Angle-of-attack ($\pm 3°$)
- CTW wing and tail angles ($\pm 5°$)
- Segment spans
- Chord and twist
- Section shape with t/c constraints
- Wing volume constraint
- BWB cabin shape constraint

- Fins are not modelled, and their drag is accounted for post-optimization

Optimization Results

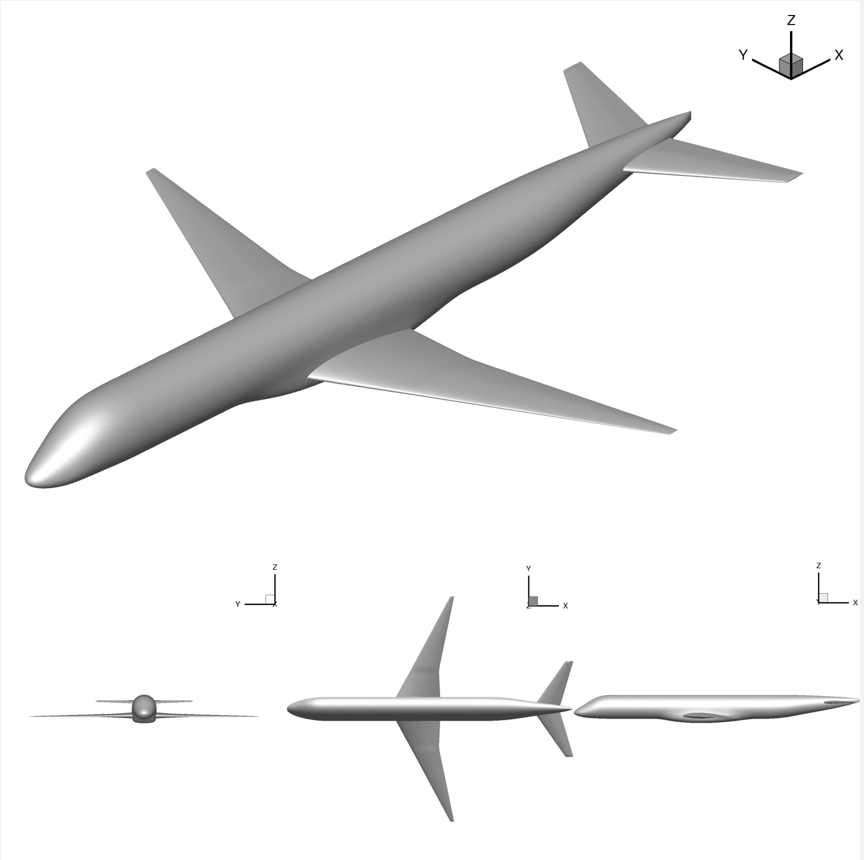

Optimized CTW100-10

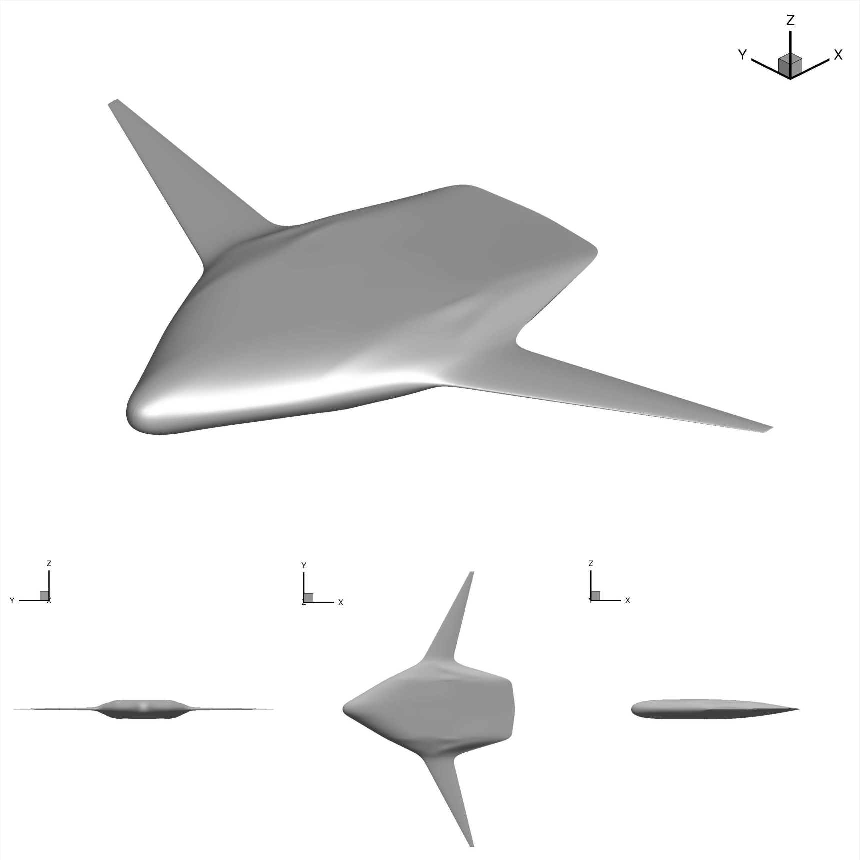

Optimized BWB100-02

$L/D = 20.0$ $\qquad$ $L/D = 21.8$

- Shock and nearly separation-free
- The BWB's wetted area is 8.4% higher than the CTW
- The BWB has 3.3% higher drag

Exploratory Result

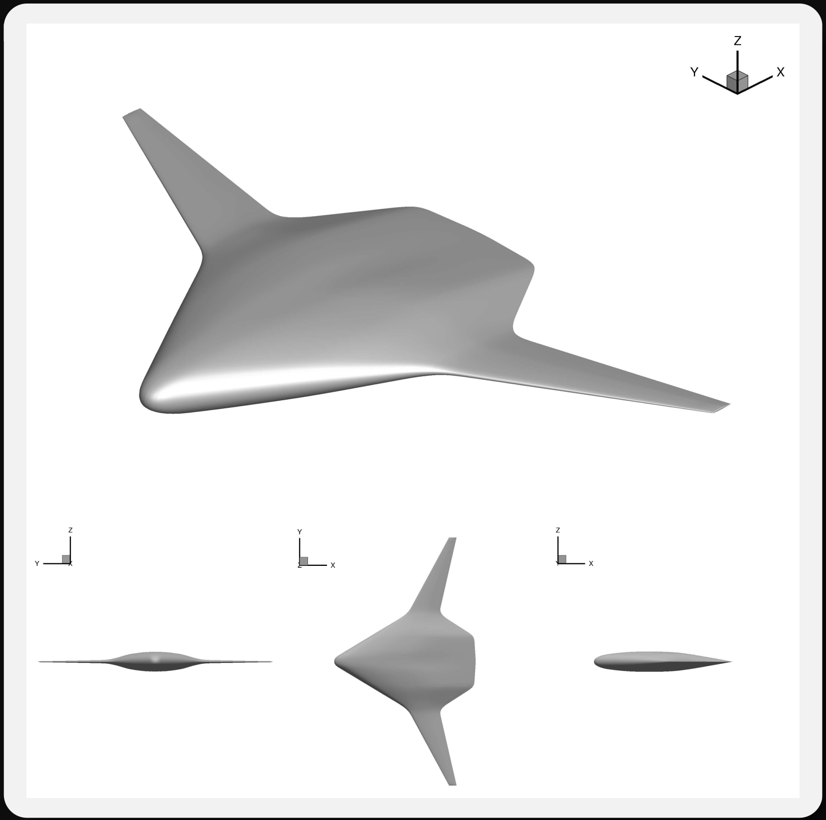

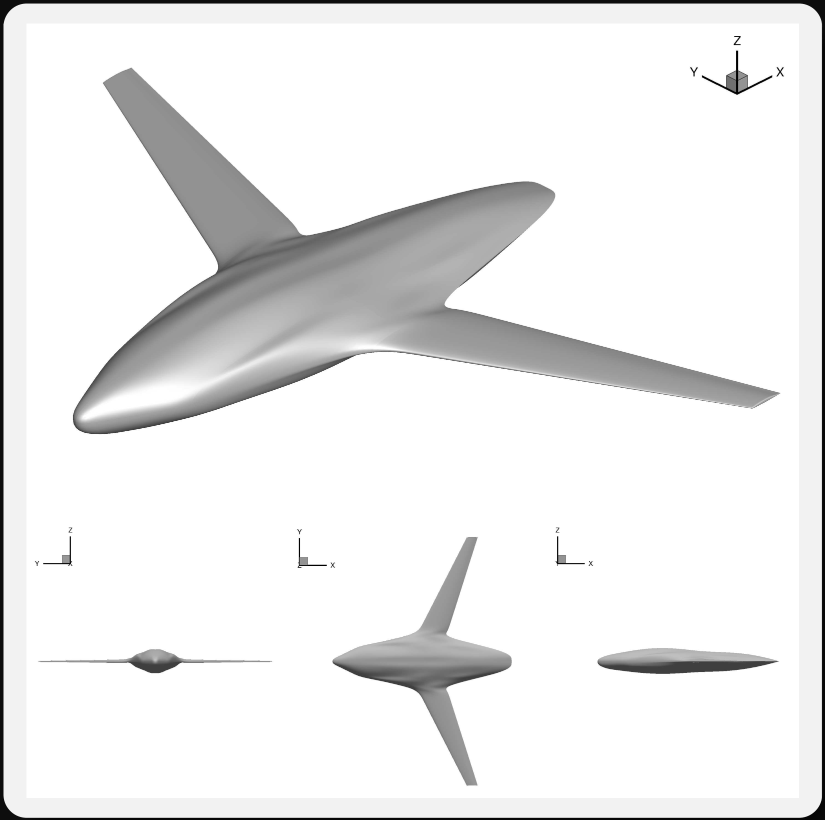

- Decreases wetted area by 10%
- Slender ‘lifting fuselage’ with a distinct wing
- $L/D = 26.1$

- Motivates the redesign and optimization of a new BWB concept

Refined BWB Design

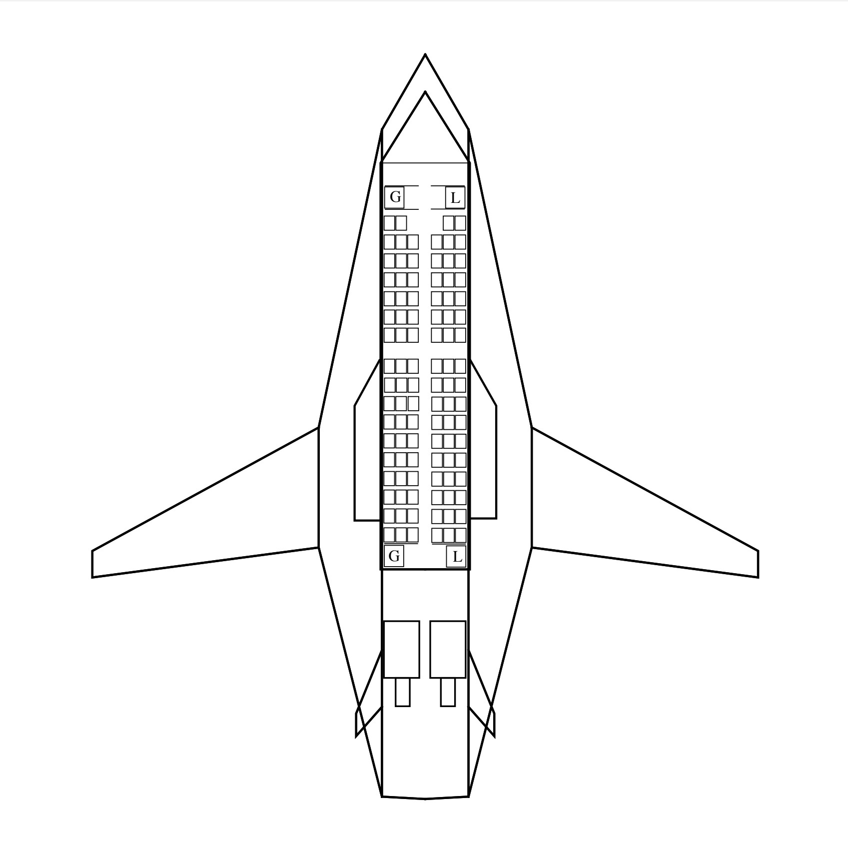

BWB100-10

Capacity		
Passengers + crew	100+5	
Max payload	28,400	lb
Geometry		
Reference area	2868	ft^2
Total span	94	ft
Length	105	ft
MAC	67.2	ft
Aspect ratio	3.1	
Weight		
MTOW	115,400	lb
OEW	65,000	lb
Wing load at MTOW	40.2	lb/ft^2
Nominal mission cruise		
Range	500	nmi
Altitude	36,000	ft
Mach number	0.78	
Reynolds number	121	$\times 10^6$
Weight*	100,000	lb
C_L*	0.17	
CG location*	54	ft

* At start of cruise

ASO of the Refined BWB Design

- Repeat the trim-constrained drag-minimization with the refined BWB
- Shock and separation-free
- Wetted area 3.6% lower than BWB100-02

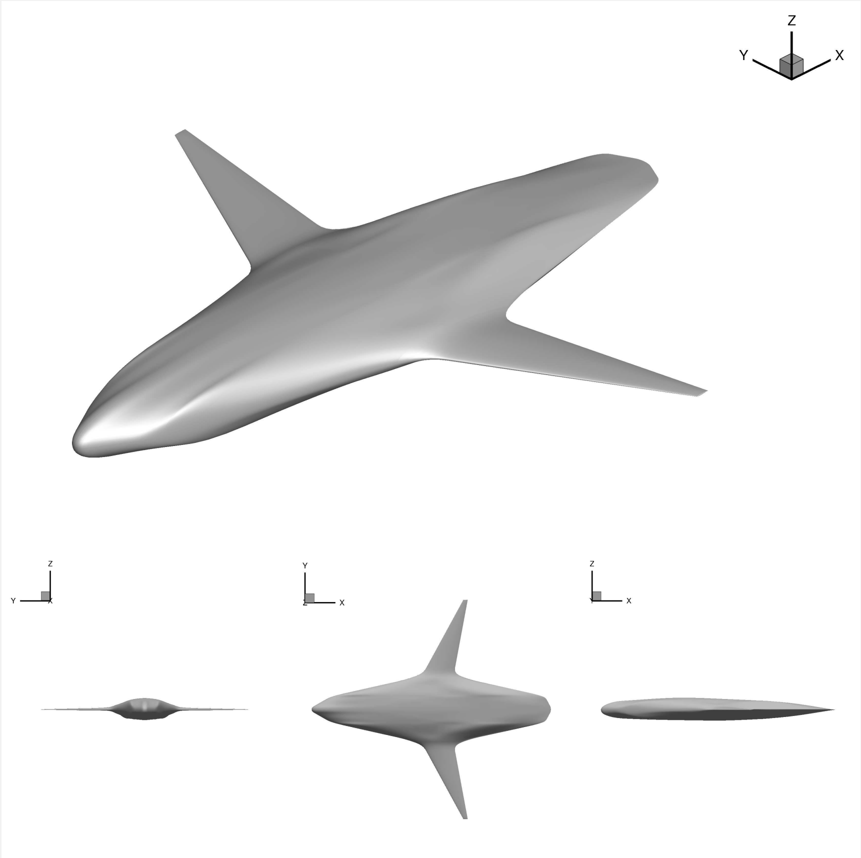

Optimized BWB100-10

$$L/D = 21.1$$

Sensitivity to Span

- For BWBs, no prior art exists for the determination of a system optimal span
- Create a second design with increased span
- Introduce the 'bending span', $b_{\text{bend}} = b - w_{\text{body}}$, as a surrogate for wing weight
- Each of these designs is optimized as before

Design	Span [ft]	Bending span [ft]	Weight* [lb]	Area [ft^2]	Wetted area† [ft^2]	L/D*† [–]	Relative drag*† [%]
CTW100-10	94	85	92,900	935	5,634	20.0	–
BWB100-02	118	76	104,600	2,732	6,286	21.8	+2.8
BWB100-03	130	88	107,700	2,813	6,444	22.6	+2.0
BWB100-10	94	64	100,000	2,535	5,922	21.1	+1.5
BWB100-12	118	88	105,000	2,674	6,189	23.9	−6.1

* At start of 500 nmi cruise
† Includes fin wetted area/drag contribution

What comes next?

- Multipoint aerodynamic shape optimization to enable robust designs and good performance over the entire flight envelope
- Multimodality can be addressed through a multi-start gradient-based approach
- If a truly promising configuration is found, then add further considerations, such as aerostructural, stability & control requirements, etc.
- Perhaps the BWB is more promising for the regional segment than previously thought